NAVAL POSTGRADUATE SCHOOL
MONTEREY, CALIFORNIA

THESIS

BURNING CHARACTERISTICS OF INDIVIDUAL ALUMINUM/ALUMINUM OXIDE PARTICLES

by

Eric C. Ruttenberg

June 1996

Thesis Advisor: David W. Netzer
Second-Reader: Oscar Biblarz

Approved for public release; distribution is unlimited.

REPORT DOCUMENTATION PAGE

Form Approved OMB No. 0704-0188

1. AGENCY USE ONLY *(Leave blank)*	2. REPORT DATE 20 June 1996	3. REPORT TYPE AND DATES COVERED Master's Thesis

4. BURNING CHARACTERISTICS OF INDIVIDUAL ALUMINUM/ALUMINUM OXIDE PARTICLES

5. FUNDING NUMBERS

6. AUTHOR(S) Eric C. Ruttenberg

7. PERFORMING ORGANIZATION NAME(S) AND ADDRESS(ES)
Naval Postgraduate School
Monterey CA 93943-5000

8. PERFORMING ORGANIZATION REPORT NUMBER

9. SPONSORING/MONITORING AGENCY NAME(S) AND ADDRESS(ES)

10. SPONSORING/MONITORING AGENCY REPORT NUMBER

11. SUPPLEMENTARY NOTES The views expressed in this thesis are those of the author and do not reflect the official policy or position of the Department of Defense or the U.S. Government.

12a. DISTRIBUTION/AVAILABILITY STATEMENT
Approved for public release; distribution is unlimited.

12b. DISTRIBUTION CODE

13. ABSTRACT *(maximum 200 words)*

An experimental investigation was conducted in which the burning characteristics of individual aluminum/aluminum oxide particles were measured using a windowed combustion bomb at atmospheric pressure and under gravity-fall conditions. A scanning electron microscope (SEM) was used to measure the size distribution of the initial aluminum particles and the aluminum oxide residue. Analysis of the residue indicated that the mass of aluminum oxide contained in particles larger than 12 microns was less than 25 percent, in good agreement with data reported from aluminized solid propellant. The measured particle size distributions and photomicrographs implied that the burning aluminum particles periodically expel aluminum oxide fragments with sizes between 14 and 36 microns.

14. SUBJECT TERMS *Aluminum Particles, Combustion Characteristics

15. NUMBER OF PAGES 48

16. PRICE CODE

17. SECURITY CLASSIFICATION OF REPORT	18. SECURITY CLASSIFICATION OF THIS PAGE	19. SECURITY CLASSIFICATION OF ABSTRACT	20. LIMITATION OF ABSTRACT
Unclassified	Unclassified	Unclassified	UL

NSN 7540-01-280-5500

Standard Form 298 (Rev. 2-89)
Prescribed by ANSI Std. 239-18 298-102

Approved for public release; distribution is unlimited.

BURNING CHARACTERISTICS OF INDIVIDUAL ALUMINUM/ALUMINUM OXIDE PARTICLES

Eric C. Ruttenberg
Lieutenant, United States Navy
B.S., United States Naval Academy, 1988

Submitted in partial fulfillment
of the requirements for the degree of

MASTER OF SCIENCE IN ASTRONAUTICAL ENGINEERING

from the

NAVAL POSTGRADUATE SCHOOL
June 1996

ABSTRACT

An experimental investigation was conducted in which the burning characteristics of individual aluminum/aluminum oxide particles were measured using a windowed combustion bomb at atmospheric pressure and under gravity-fall conditions. A scanning electron microscope (SEM) was used to measure the size distribution of the initial aluminum particles and the aluminum oxide residue. Analysis of the residue indicated that the mass of aluminum oxide contained in particles larger than 12 microns was less than 25 percent, in good agreement with data reported from aluminized solid propellant. The measured particle size distributions and photomicrographs implied that the burning aluminum particles periodically expel aluminum oxide fragments with sizes between 14 and 36 microns.

TABLE OF CONTENTS

LIST OF SYMBOLS

D	Agglomerate diameter prior to nozzle
D_{ag}	Agglomerate diameter
d_p	Characteristic diameter of the drop
l	Characteristic length
On	Ohnesorge number (viscous tension/surface tension)
t	Time in seconds
v	Relative velocity between flowfield and drop
We	Weber number
We_{cr}	Critical Weber number
α_k	Mole fraction of oxidizing species
β	Fractional size of aluminum agglomerate particle
μ_d	Dynamic viscosity of the drop
ρ	density of the flowfield
ρ_d	density of the drop
σ	Surface tension
τ	Particle burning time

I. INTRODUCTION

Aluminum particles are used in composite or composite-modified double-base rocket propellants to provide the intense heat release of aluminum combustion, increasing specific impulse as well as enhancing acoustic stability and propellant density. Typical solid propellants use aluminum (up to 22 percent by weight) as a fuel and ammonium perchlorate (AP) as an oxidizer. Aluminum is inexpensive, readily available, non-toxic, nonreactive during propellant processing and storage, and compatible with propellant processing (Price, 1982). The unique combustion behavior of aluminum is due to the physical and thermochemical properties of metals and their oxides, which have high densities and high heats of reaction (Price, 1984).

There are several basic processes involved in the combustion of an individual aluminum particle. Following an inert heating process, the aluminum particle ignites and eventually becomes an aluminum oxide particle. Before ignition aluminum particles typically have an oxide layer approximately one micron thick. This layer inhibits ignition until it melts, exposing the aluminum. The actual time of ignition is not well defined, but the process following the observance of a bright droplet is important because it affects particle breakup and final particle size. The temperature of the aluminum droplet during combustion is approximately 2500° K and the gas in the flame region is typically as high as 3800° K. A sketch of a typical burning aluminum particle in the motor environment is found in Figure 1.

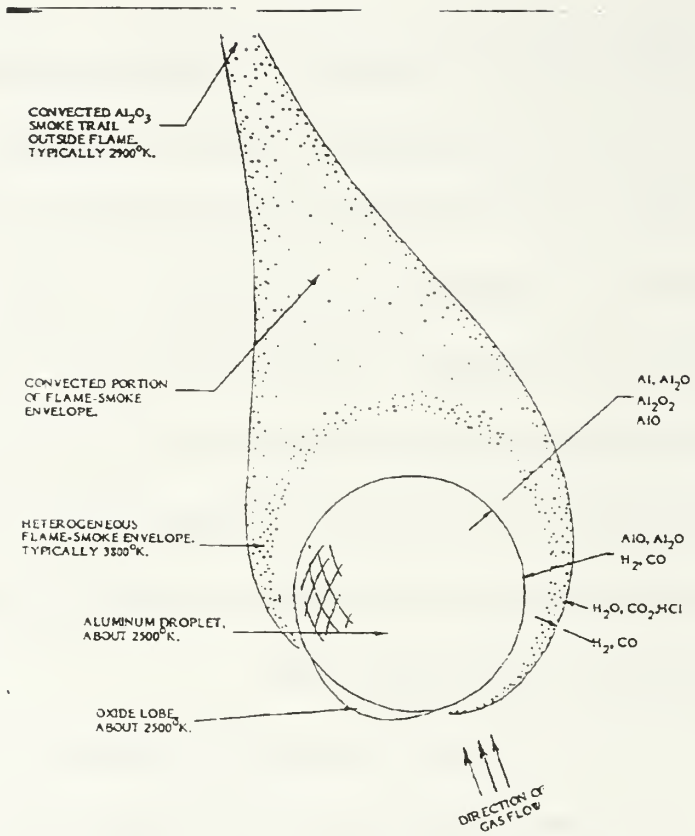

Figure 1. Sketch of a typical aluminum agglomerate during combustion (Price, 1984, pp. 479-513).

Surface oxide, formed primarily by the presence of H_2O, becomes a dominant part of combustion as burning progresses. In almost all studies of droplet combustion, an appreciable amount of oxide is found on the droplet burning surface. The burning rate of an agglomerate is important when determining conditions that might lead to incomplete combustion in the motor and for determining the particle sizes for dampening oscillatory disturbances. The burning time for an aluminum droplet is dependent on initial particle

diameter, mole fraction of the oxidizing species, and pressure and is in the form (Price , 1982)

$$\tau \propto kD^n \tag{1}$$

where n is a value between 1.5 and 1.75, and a corresponding value of k being (for n=1.5)

$$k = 6.7 \times 10^{-3} \Big/ \alpha_k^{0.9} \tag{2}$$

The constant 6.7×10^{-3} is a function of pressure, oxidizer properties, and a weak function of atmospheric temperature. (Price, 1982) Figure 2a shows aluminum droplet burning times as a function of diameter. Droplet burning rates are often found to approximately follow a d^2-law, e.g., $D^2 = D_o^2 - Kt$, where D_o is the initial diameter and K is the evaporation constant. This behavior is shown in Figure 2b. However, it is apparent that K varies for different propellants.

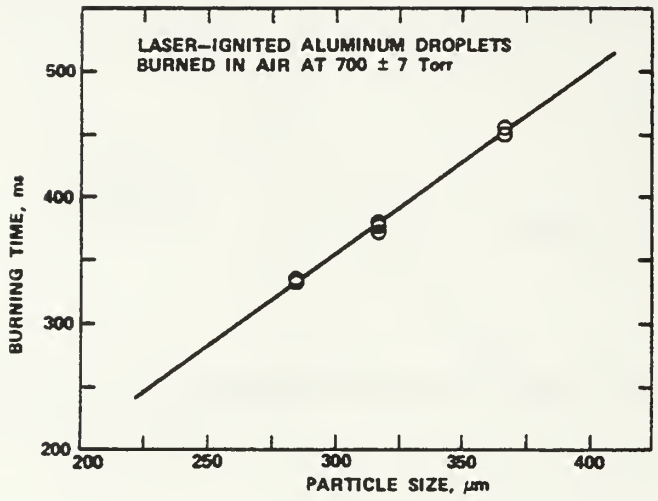

(a)

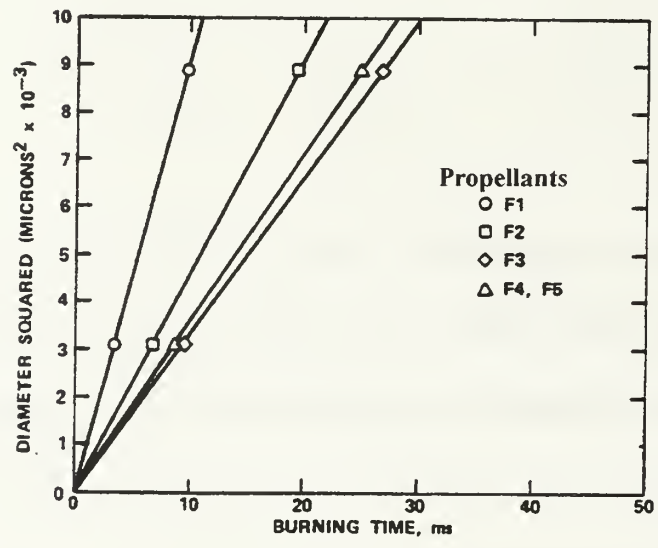

(b)

Figure 2. Burning time of aluminum droplets: (a) Laser ignited aluminum droplets burning in air; (b) Measurement in a propellant product atmosphere for five propellants (Price, 1982, p. 107).

In a solid propellant rocket motor the aluminum particle experiences a variety of environments and flow conditions. As the particles reach the burning propellant surface they melt and may join with other particles to form large agglomerates. When they leave

the propellant surface the heavy oxide lobe which was on the top of the agglomerate generally results in the rotation of the lobe to the bottom as shown in Figure 1. The particle/agglomerate continues to burn as it passes through the combustor towards the exhaust nozzle. Its trajectory will depend upon both its injection point from the surface and its size. In this region collisions may lead to particle size growth due to coalescence or particle size reduction due to breakup.

Larger particles will be unable to follow the gas flow around a submerged nozzle and, therefore, can accumulate as slag. The slag gathers behind the submerged nozzle and can alter motor performance due to excessive heat transfer, failure to expel all propellant mass, and/or pressure fluctuations from periodic passage of slag through the nozzle. Prior to 1988 there was little particle size distribution data for model validation, and slag models predictions varied greatly (Salita, 1995). Since 1988 measurements of droplet size distributions have been conducted for numerous propellants, yet there remains disagreement on the distribution of particles and there maximum diameter. Slag accumulation studies presented by Salita and discussed at the JANNAF workshop (Salita, 1994) agree that slag accumulates somewhere behind the nozzle nosetip depending on nozzle/web geometry and motor burn time. However, particle size distribution remains an issue which has not been resolved. While larger particle sizes are known to cause slag build up, there is disagreement as to the mass-median diameter that causes slag accumulation.

As the particles of aluminum and/or aluminum oxide approach the nozzle throat, they gain velocity, change in temperature, and may change in size due to collision

coalescence and/or breakup at the critical Weber number. Experimental observations have revealed that the terminal phase of burning can be both complex and varied. The ratio of the inertial forces to the surface tension forces, known as the Weber number, predicts reasonably well the breakup behavior of agglomerates and droplets through the nozzle. The classical definition for the Weber number is the product of the square of the fluid velocity relative to the particle, the density of the fluid, and the characteristic length divided by the surface tension:

$$We = v^2 \rho l / \sigma \tag{3}$$

Bartlett and Delaney (1966) based a model for particle breakup on the critical Weber number. Pilch and Erdman (1987) used data from impulsive-lag breakup experiments to define the Weber number based on the Ohnesorge number as:

$$We_{cr} = 12(1+1.077On^{1.6}) \tag{4}$$

$$O_n = \mu_d / (\rho_d d_p \sigma)^{0.5} \tag{5}$$

It is known that for small Weber numbers the particle shapes are spherical, and for Weber numbers of approximately four the particles begin to distort. It is not until the flow approaches Weber numbers of 20 to 30 (Caveny, 1979) that the agglomerates break up to form multiple smaller agglomerates. In solid propellant rocket motor combustion chambers the Weber number generally will not reach the critical value, therefore this

mode of breakup is not expected to occur until the nozzle is reached. According to Pilch (1987) liquid droplets can experience bag breakup between Weber numbers of 12and 50 which can be related to the values of 20-30 by Caveny. Figure 3 illustrates particle distortion and breakup as a function of Weber number.

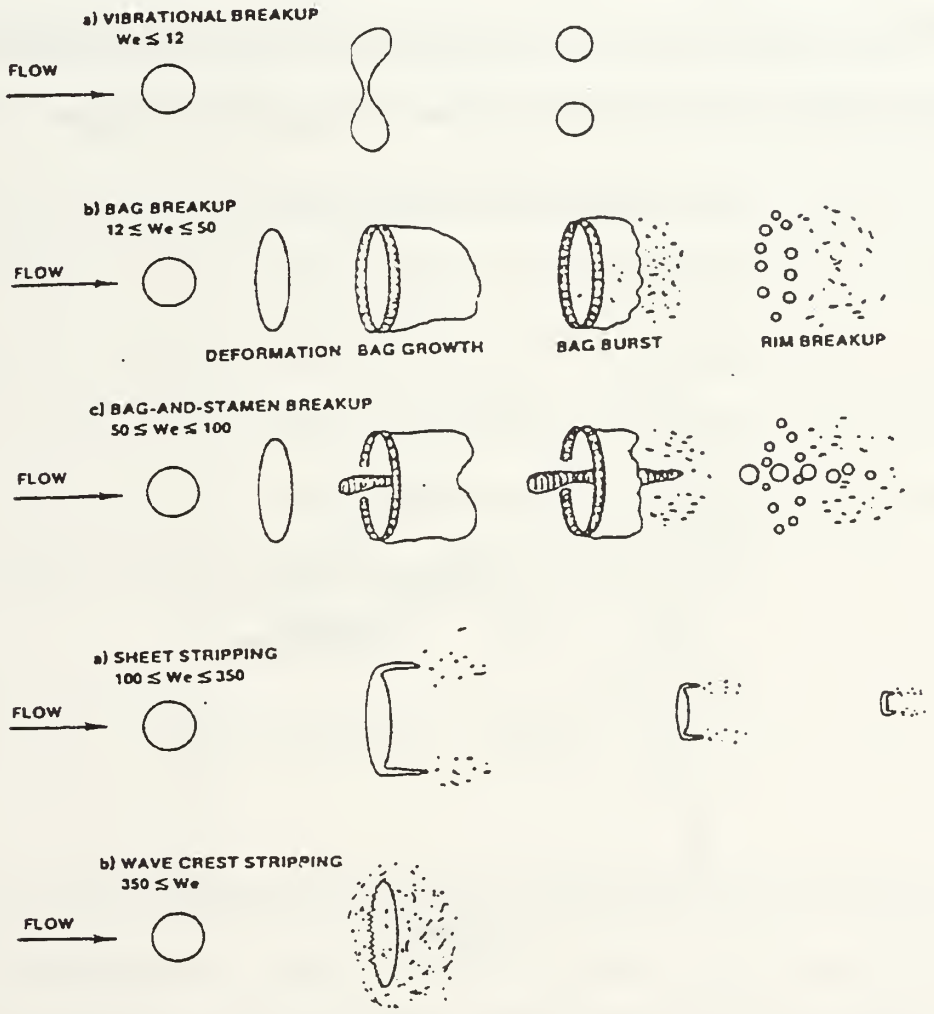

Figure 3. Observed variation of impulsive breakup scenarios with Weber number (Bartlett, 1966, pp. 337-341).

In addition to Weber number, characteristic breakup time determines if a breakup will occur in a given flow situation (Caveny, 1979). These particle breakup models imply a dependence on chamber pressure and nozzle throat diameter. An agglomerate breakup usually occurs at a critical Weber number which is achieved by the time the particle reaches the throat of the nozzle. Larger agglomerates reach the critical Weber number early in the nozzle entrance flow process as the velocity differential of the gas and particles reach approximately 10 to 1 (Caveny, 1979). The relationship of velocity differential and Weber number is shown in Figure 4 for various particle sizes.

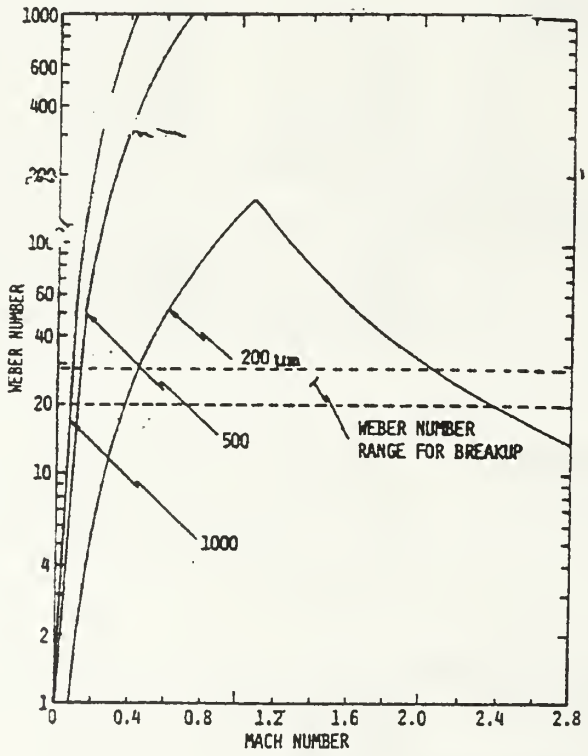

Figure 4. Variation of Weber number for a range of agglomerate sizes entering the nozzle (Jenkins, 1969).

Previous works by Salita (1994), Bloomshield (1994), Laredo (1994), and Gomes (1994) present particle size distributions obtained in combustion bombs and subscale motor chambers. Salita, Bloomsfield, and Laredo investigated collected residue of Shuttle Booster solid propellant (TP-H1148) while Gomes summarized aluminum and aluminum oxide particulate data from a wide range of propellants burned in small-scale motors. Figure 5 compares the size distribution from the four investigations.

Salita's work divided the collected particles in a quench-bomb into two main categories. Particles smaller than 25 microns were classified as smoke, and particles ranging from 50 to 130 microns were classified as caps. Smoke represented 70 to 80 percent of the mass of the residue collected with a mass mean diameter of 1.5 micron. Salita determined that 50 percent of the smoke mass was smaller than 1.5 micron, 90 percent was smaller than 5 micron, 99 percent was smaller than 10 micron, and 99.9 percent of the smoke was smaller than 25 micron. The final mean size of the remaining caps (D) could be predicted using the expression

$$D = \beta D_{ag} \tag{6}$$

where β is a value between 0.55 and 0.80 and D_{ag} is the initial agglomerate diameter.

Bloomshield, et.al., collected TPH-1148 propellant particle data using a dry combustion bomb with three different ammonium perchlorate manufacturers. The results noted in these experiments were different from Salita's in that 80 percent of the collected particle mass was in particles smaller than 5 microns versus 63 to 72 percent

for the Salita data, and only 4 percent of the particle mass had diameters greater than 25 microns versus 20 to 30 percent for the Salita data.

Laredo, using optical methods during motor firings with the same type of propellant came up with very similar data to Bloomshield. While Laredo points out that approximately 80 percent of the particle mass was between 4 and 9 micron, and the remaining 20 percent was smaller than approximately 4 microns, it was also determined that 80 percent of the particles were smaller than 7 micron (versus 5 microns in the Bloomshield data), and no particles were measured larger than 25 microns.

Gomes' summary of all types of aluminized propellants fired in a subscale motor concludes that particles less than 5-10 microns generally comprise 80 percent of the volume, particles greater than 5-10 microns provide approximately 20 percent, and that there is less than 20 percent of the volume in particles greater than 25 microns. These results are nearly identical to the results of Bloomshield, but differ from the results of Salita and Laredo. Figure 5 implies that the optical measurements made by Laredo through the subscale combustor were unable to detect the relatively few number of large particles that comprise approximately 5-20 percent of the particle mass.

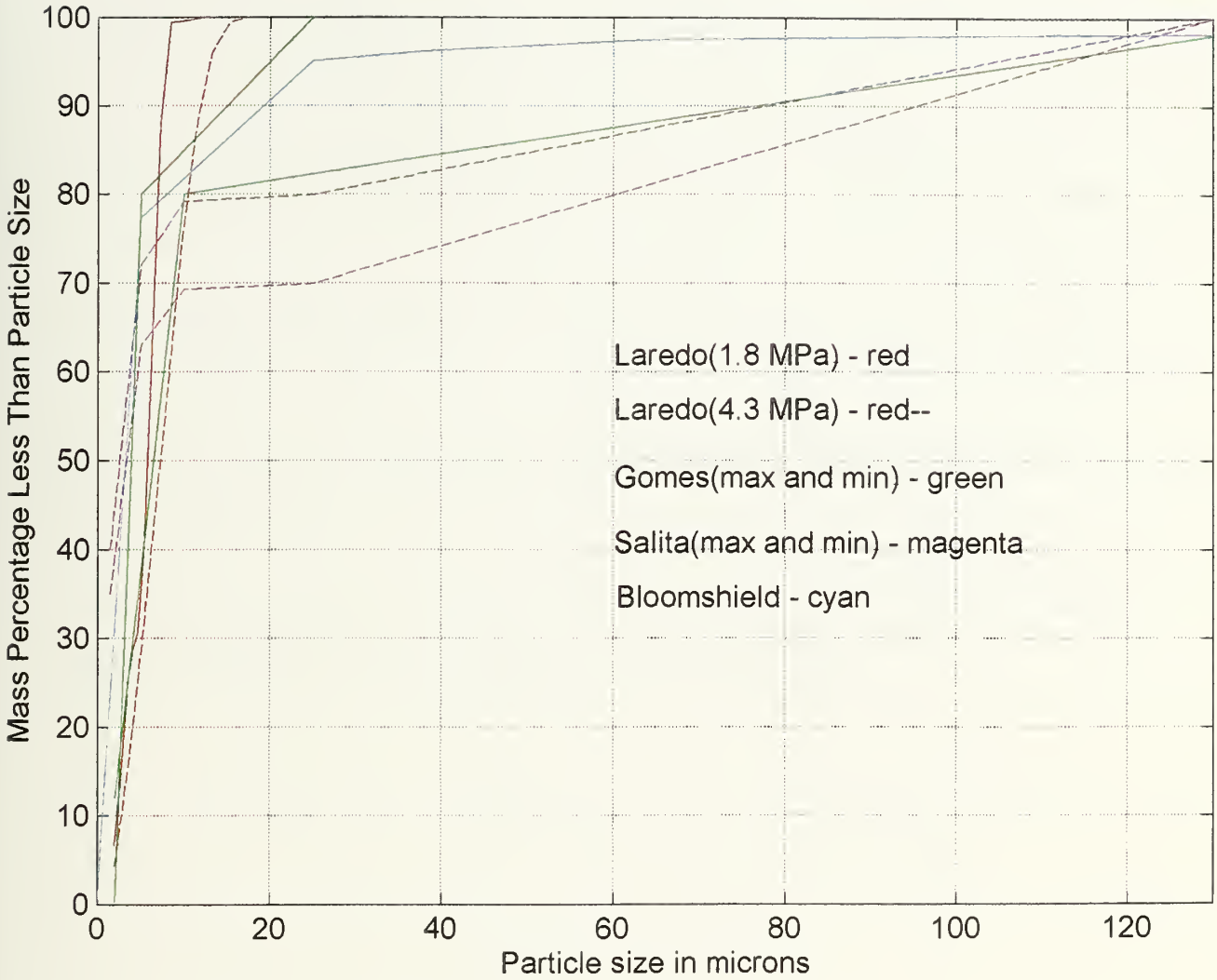

Figure 5. Particle size distribution of aluminum/aluminum oxide particles collected by Laredo, Gomes, Salita, and Bloomshield.

The wide variation in the particle sizes reported above could possibly result from the variation in particle sizes leaving the propellant surface, but no such correlation has been published. Thus, individual particle burning characteristics are unknown. Only the "average" behavior based on mean diameters can be surmised. It is also possible that a particle breakup mechanism, other than that of exceeding the critical Weber number,

exists under motor operating conditions as postulated by Gomes. The studies referenced above also indicate that there exists a bimodal or trimodal distribution consisting of monomodal or multimodal smoke and aluminum oxide caps, yet they do not provide a comprehensive explanation for this distribution. Individual particle experiments in the past have used levitated particles to examine burning characteristics. This technique does not provide a realistic "motor condition", e.g., burning particles moving with increasing velocity and random paths. In this investigation individual particles with a narrow range of initial sizes were ignited and permitted to burn to completion while falling under the influence of gravity in order to determine if particle breakup occurs under the low velocity conditions present in combustion chambers.

II. METHOD OF INVESTIGATION

A windowed combustion bomb was modified to provide the ability to laser-ignite solid particles under atmospheric conditions. Aluminum particles between 88 and 105 microns entered the combustion bomb through a syringe where they were ignited on opposites sides by a CO_2 laser operating at 60 Watts power. The 4 millimeter laser beam was focused down to a 0.15 millimeter diameter, producing a radiant flux density of approximately 15 kilowatts per centimeter squared. Particles passing through or in close proximity to the focal point were ignited and allowed to free-fall.

Burn time and the final particle size distribution were determined using two techniques; a video camera of the burning process and photomicroscopy of quenched particles. Experiments were conducted at 1 ATM. The final particle sizes were compared to empirical correlations and empirical data contained in the literature in order to determine if particle breakup could occur under the low velocity conditions typical in solid propellant motor chambers.

III. EXPERIMENTAL APPARATUS

A. ALUMINUM PARTICLES

The H-95 approximately spherical aluminum particles used for this study were provided by Valimet Incorporated. They were sifted through mesh strainers to ensure that all the particles were between 88 microns and 105 microns. A random sample was measured using a SEM to determine the nominal size distribution and particle appearance prior to particle ignition.

B. COMBUSTION BOMB

All of the experiments were conducted using a widowed, stainless steel combustion bomb. The circular bomb stands 19 inches tall and 4.7 inches wide. A one-inch diameter bore running lengthwise 14.75 inches allows falling particles to completely burn under various atmospheric pressures and chamber velocities. There are two 12-inch long observation windows made of Plexiglas running the length of the chamber. The windows provide the capability to use a background lighting source and video equipment. The windows also prevent air currents in the room from affecting the particle trajectory both before and after particle ignition. This was extremely important because the sizes of the aluminum particles were only 40 to 80 microns smaller than the laser beam width at its focus.

The aluminum particles were stored in a small chamber with a 22 gauge stainless steel hypodermic needle located at the bottom. The chamber was connected to a three-axis micrometer stage to allow placement of the needle directly over the beam center and as close as possible. This greatly enhanced the probability of particle ignition by reducing the particle acceleration due to gravity, increasing the time the particle was exposed to the beam. Low frequency vibrations external to the chamber were used to cause the particles to randomly enter the needle, allowing single particle evolutions. The needle had an inside diameter of 240 microns, large enough to permit two particles to occasionally enter simultaneously, but prohibiting two particles from blocking the needle exit. Larger needles lead to multiple particle evolutions and smaller diameter needles were easily blocked. The relatively large needle diameter also allowed the particles to enter the chamber in a near free fall state, without any added velocity. This is significant when using a high shutter speed camera to determine path trajectory.

Two side windows on the bomb were used to illuminate the aluminum particles as they exited the needle approximately one hundred microns above the beam. The side windows were made of zinc-selenide. These windows are required to conduct non-atmospheric experiments and to transmit the 10.6 micron wavelength from the CO_2 laser. Zinc selenide is unique in its ability to transmit large amounts of energy without changing temperature or absorbing the light source. The combustion bomb is depicted in Figure 6.

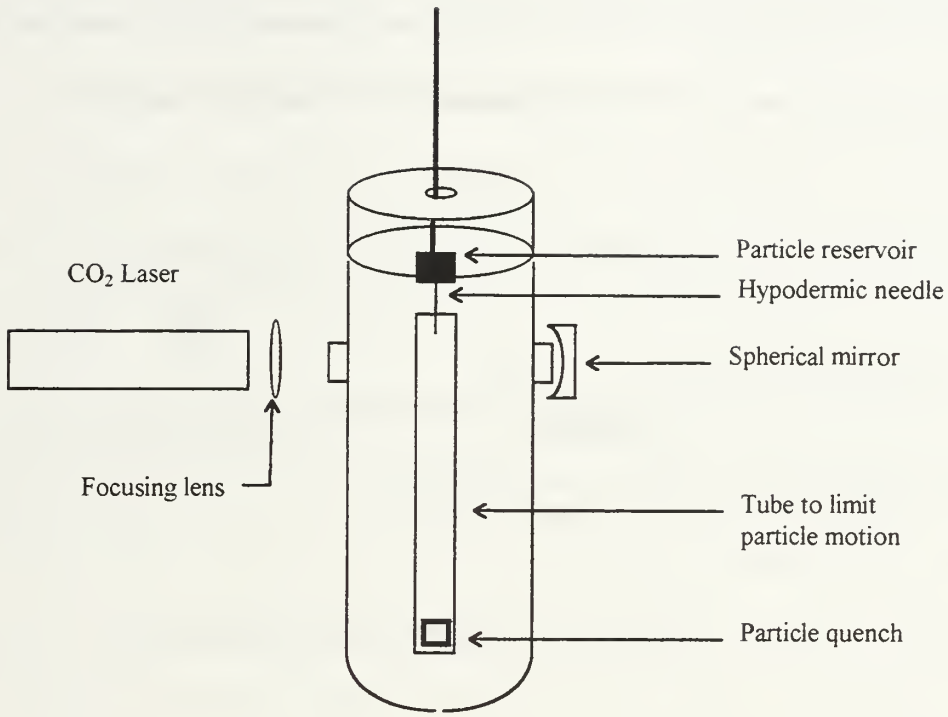

Figure 6. Schematic of the windowed combustion bomb.

C. PARTICLE IGNITION

The aluminum particles were ignited using a focused CO_2 laser beam. Using a zinc-selenide plano-convex lens with a focus of 5 inches, the beam was narrowed to a 0.15 millimeter waist diameter directly under the hypodermic needle. As the beam exits the bomb on the right side, it is reflected back along the same path using a silicon spherical mirror which has a focal length of 2.5 inches. Mirrors of this type are considered to reflect 99.5 percent of the 10.6 micron wavelength and handle up to several kilowatts of power. To prevent damage to the mirror, the laser was limited to fifty

percent power (60 Watts). By reflecting the beam back into the chamber the particle is ignited on both sides. A schematic drawing of the laser setup is found below.

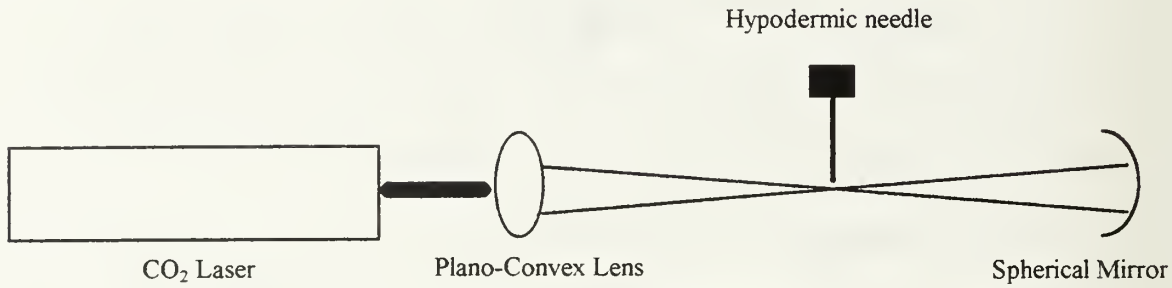

Figure 7. CO_2 Laser and optics diagram.

D. DATA EXTRACTION

1. Cameras

Particle diameter measured by the width of the burning particle trail was attempted with the use of two video cameras, looking through the front and back of the combustion bomb windows. During experiments the work space was darkened allowing the ignited aluminum particles to provide the necessary lighting for the video cameras. An inadequate number of pixels were available to measure the particle diameter with the magnification employed, but the videos continued to provide reliable streak data. Ultimately, the video data were used to determine when the particle had finished burning. The video input signal was fed from the work space into a VCR together with signals

from two annotators. One annotator produced a visible time signal with the date and time in 100 microsecond intervals. The other annotator provided text. Following several runs where good data were taken, the video pictures where transferred to the computer using the Vidcapture frame program. The data in the computer were then viewed using a bit-edit program.

The two video cameras used were a studio type Panasonic WV-F300 series color video camera and a Computar BCE-3900 series black-and-white camera. Both cameras collected data at 30 frames per second. The Computar camera had a better resolution and was used to look at the particles exiting the needle. The drawback of this camera was its extremely limited field of view. The color camera had a wide field of view, worse resolution, but a electronic shutter speed variable from 1/250 up to 1/1000 seconds. This camera was used in conjunction with a fresnel lens to record the particle streaks following their ignition.

2. Particle Quench

The aluminum particles were quenched after burnout inside the combustion bomb. The particles were collected in two ways. A dry-quench and a water-ethanol quench were used to determine the possible effects of the quenching process on the measured particle sizes. The copper quench platform was initially established at a point where the particles had already extinguished as determined from the video camera streak

images. Figure 8 shows a typical particle streak. Although particle combustion was complete just above the quench platform the particles would still be molten.

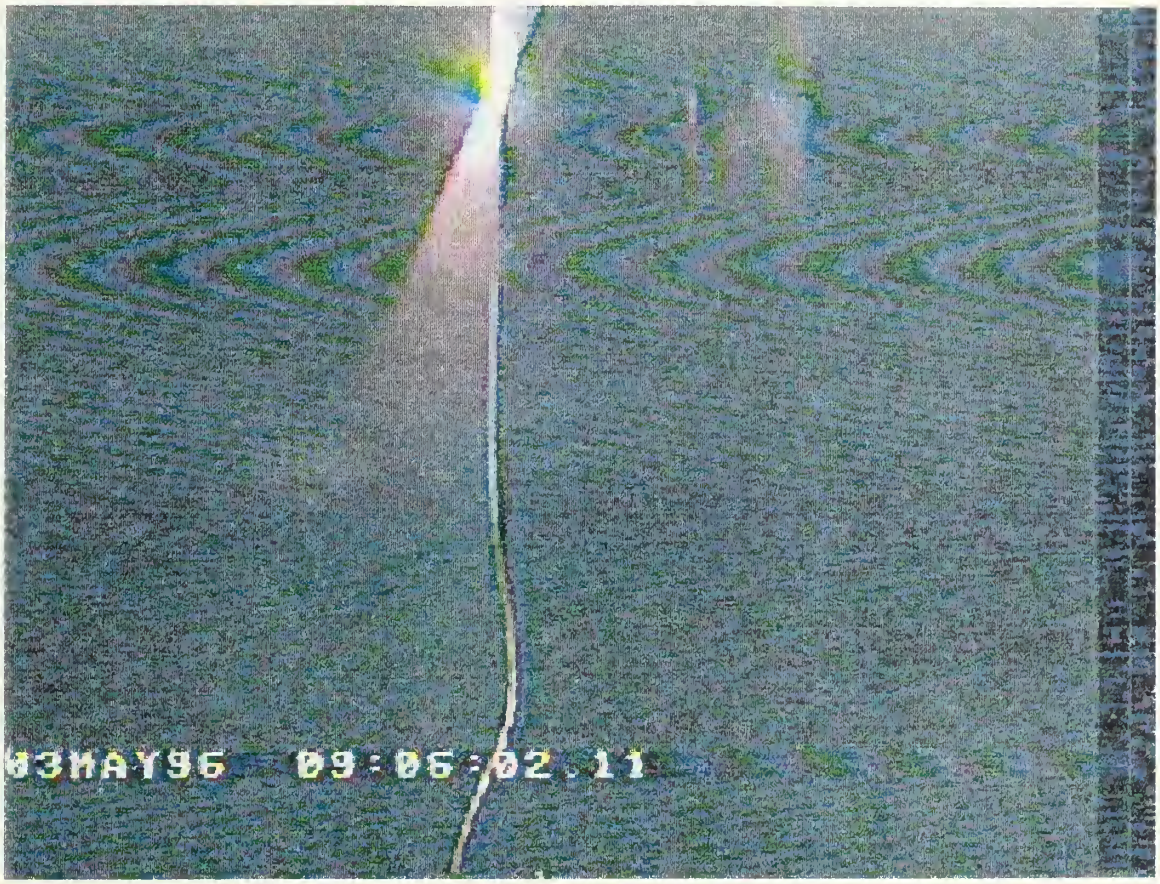

Figure 8. Particle streak data signifying completion of burn time.

The quenched samples were mounted on pedestals and examined under a SEM to determine individual diameters, and diameter distribution. Particles which were smaller than 50 percent of the initial particle size (minimum expected β, equation (6)), but larger than the one to ten micron smoke particles were considered to have experienced particle breakup.

IV. RESULTS

Table 1 presents the data obtained for the raw aluminum particles using an SEM and a sample size of 200. Figure 9 shows the size distribution of the raw particles by presenting the percentage of raw particles within two micron bands. It should be noted that particles existed which were larger than the mesh screen. This was due to elongated particles found in the sample obtained from Valimet Inc. The average particle size was 98 microns. Using this nominal particle size, the final particle diameter of the aluminum oxide caps should be between approximately 55 and 79 microns. However, due to the variation in initial particle diameters, the final oxide cap sizes could be as small as 42 microns.

Diameter μm	Percent	Cumulative Percent	Diameter μm	Percent	Cumulative Percent	Diameter μm	Percent	Cumulative Percent
<76.9	1.0	1.0	94	5.0	39	110	4.0	93
80	2.0	3.0	96	7.0	46	112	1.0	94
82	3.0	6.0	98	11	57	114	0	94
84	1.0	7.0	100	9.0	66	116	0	94
86	6.0	13	102	10	76	118	2.0	96
88	6.0	19	104	2.0	78	120	0	96
90	9.0	28	106	7.0	85	122	1.0	97
92	6.0	34	108	4.0	89	141	3.0	100

Table 1. Measured Particle Size Distribution of Raw Aluminum Particles.

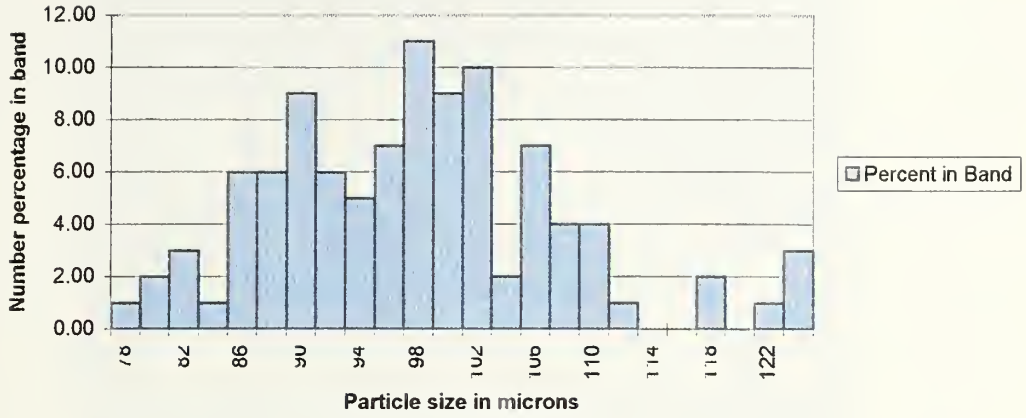

Figure 9. Distribution of Raw Aluminum Particles in Two Micron Bands.

Figures 10 and 11 show photographs of the raw particles. Figure 10 shows that the majority of the aluminum particles were nearly spherical, with several particles being oblong in shape. Figure 11 shows that the particles had a rough oxide surface and a number of smaller particles attached.

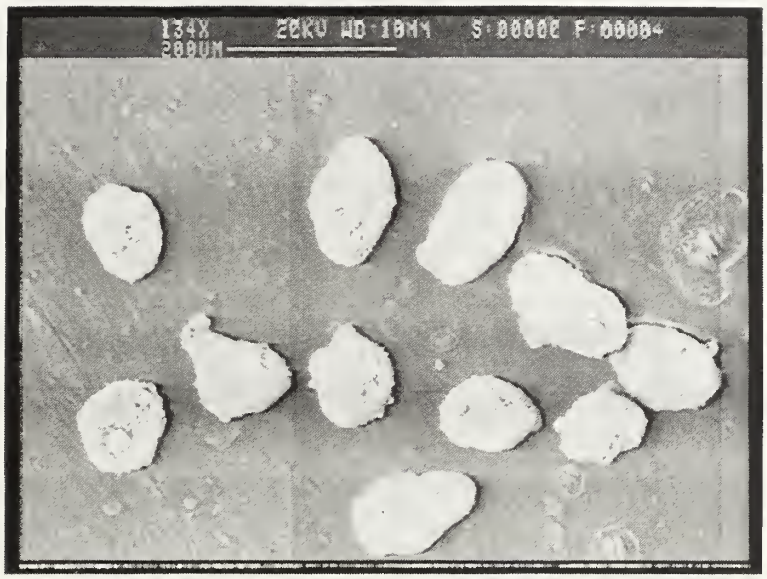

Figure 10. SEM image of raw aluminum particles between 80 and 115 microns.

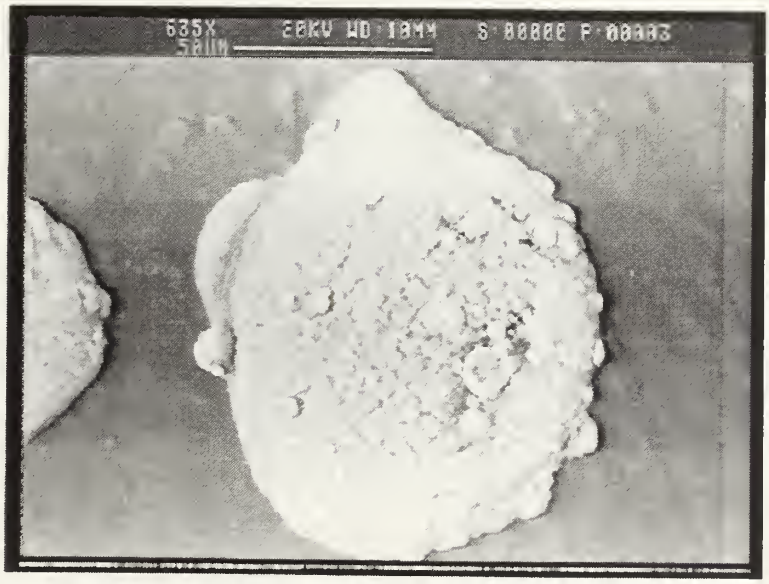

Figure 11. SEM image of single aluminum particle prior to laser ignition.

The collections of quenched particles were examined using the SEM to determine if particle breakup had occurred for a slowly accelerating particle during combustion. Without combustion, the free-falling particle would have reached a terminal velocity at the quench platform of 1.9 m/s.

Table 2 lists the measured particle sizes ≤ 12 microns in diameter ("smoke"), their percentage of the total distribution, and the cumulative percentage, all from the burning of one aluminum particle. It should be noted that not all the smoke would reach the quench plate. Some would deposit on the inside of the tube connecting the ignition location to the quench plate. Figure 12 presents the cumulative number distribution for the smoke particles. Figures 13 and 14 display the number and volume distributions of the "smoke" particles, respectively. The number distribution was approximately Gaussian. The volume distribution was constructed assuming that all of the smoke particles had the same density and was bimodal or trimodal in agreement with the data of Laredo (1994).

Diameter μm	Percent	Cumulative Percent	Diameter μm	Percent	Cumulative Percent	Diameter μm	Percent	Cumulative Percent
0.50	1.08	1.08	4.50	1.49	92.65	8.50	0.50	98.94
1.00	19.37	20.45	5.00	1.90	94.55	9.00	0.25	99.19
1..50	23.18	43.63	5.50	1.32	95.87	9.50	0.17	99.36
2.00	23.68	67.31	6.00	0.83	96.70	10.00	0.00	99.36
2.50	10.93	78.24	6.50	0.75	97.45	10.50	0.17	99.53
3.00	7.95	86.19	7.00	0.58	98.03	11.00	0.25	99.78
3.50	1.99	88.18	7.50	0.33	98.36	11.50	0.00	99.78
4.00	2.98	91.16	8.00	0.08	98.44	12.00	0.25	100.0

Table 2. Measured particle size distribution of smoke particles (1209 total particles).

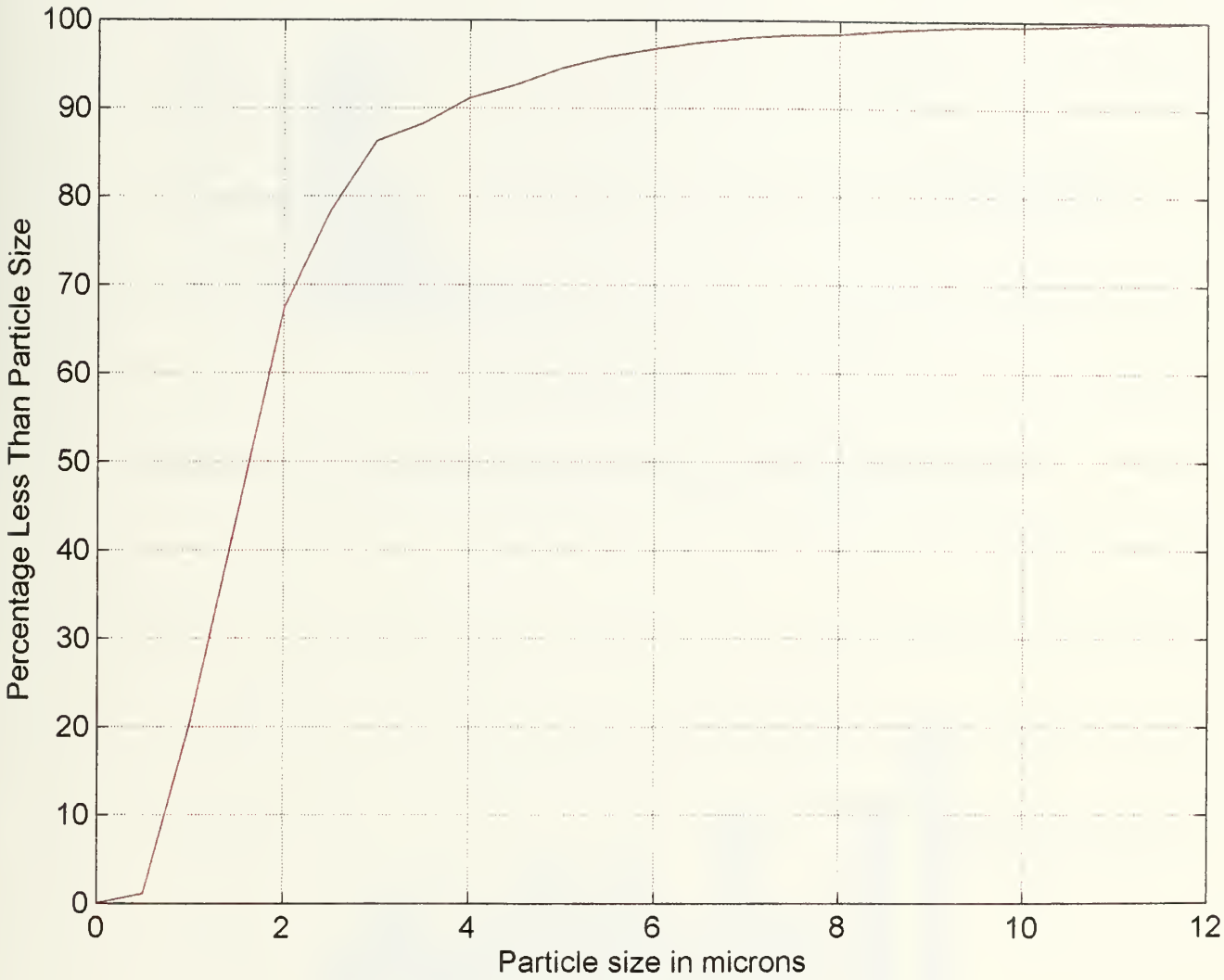

Figure 12. Particle size distribution of aluminum/aluminum oxide "smoke" particles collected from one particle using a dry quench.

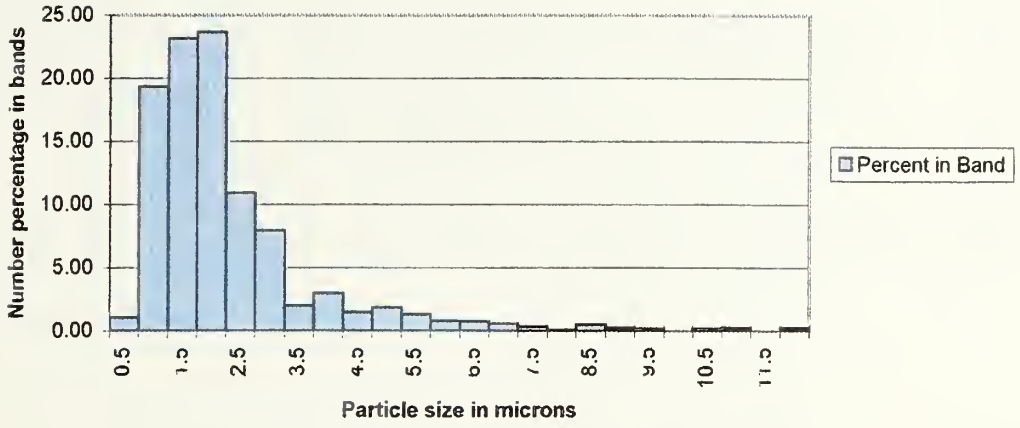

Figure 13. Smoke particle number distribution in 0.5 micron bands.

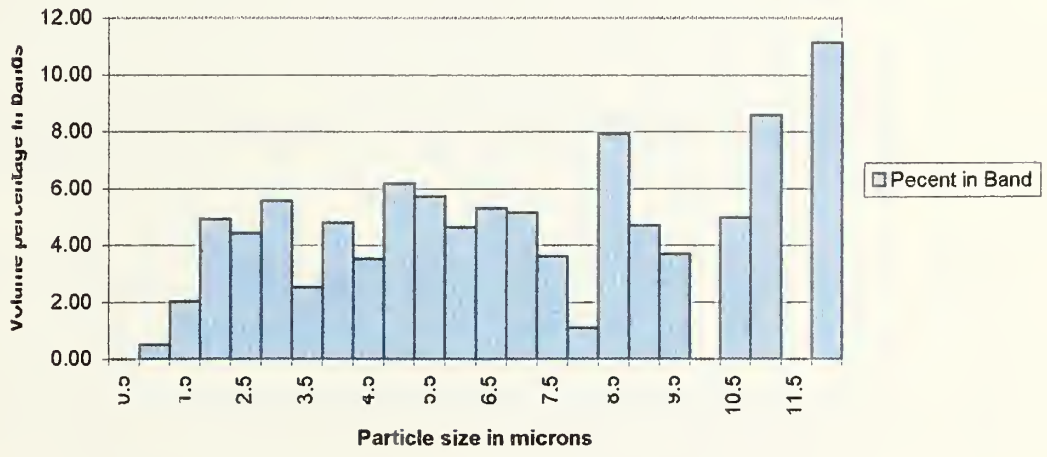

Figure 14. Smoke particle volume distribution in 0.5 micron bands.

The smoke particles observed on all of the pedestals appeared more spherical as the size of the particle decreased. The smoke particles obtained using the water/methanol quench had essentially the same characteristics.

Using the same pedestal as was used to acquire smoke data, particles larger than 12 microns were measured and tabulated to determine if particle breakup was occurring at atmospheric conditions under gravitational acceleration. The data in Table 3 are only for particles that were too large to be labeled as smoke particles. Several of the particles collected were elongated which implies that particles may have collided when quenched to produce larger particles.

Mean Diameter μm	Number of Particles	Mean Diameter μm	Number of Particles
14	3	30	1
16	3	32	1
18	2	34	1
20	1	42	2
22	3		

Table 3. Measured particle sizes of larger aluminum/aluminum oxide particles.

If the aluminum particle had a mean diameter of 98 microns and was converted to Al_2O_3 then the total aluminum oxide mass produced would be 2.52×10^{-6} grams. If all of the collected residue were assumed to be solid oxide the particles with diameters greater than 12 microns (Table 3) would account for approximately 25 percent of the total mass. Of course, if the particles are porous or hollow they would account for a smaller percentage of the total mass. Porous aluminum oxide can have a density one-half that of solid aluminum oxide. In that case the large particles would account for less than 12

percent of the total mass. The 25 percent value is in good agreement with the data shown in Figure 5.

To determine the possible effects of the quenching method on the larger aluminum/aluminum oxide particles/caps, those quenched by the water/methanol solution were also measured. These particles appeared (as expected) to have gone through a much faster cooling process causing large cracks in the surfaces of the particles. The dry quenched particles which were 14-36 microns in mean diameter (see Figure 15) appeared to be more jagged and less spherical than the comparable liquid quenched particles (see Figure 16). However, the general shapes of the liquid quenched particles were very similar to those of the dry quenched particles. The particles between 14 and 36 microns were most often jagged and somewhat elongated whereas the particles larger than 42 microns were generally smoother and more spherical.

Figure 15. Dry quenched particle illustrating jagged features and elongated shape.

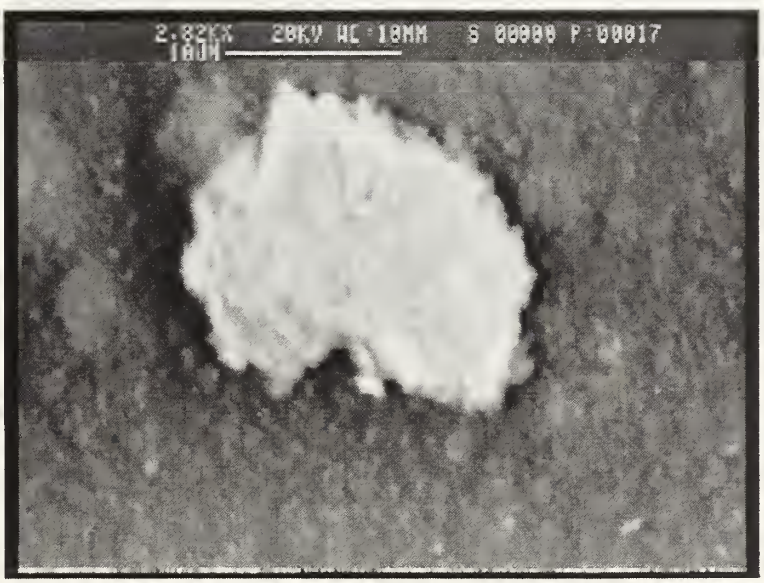

Figure 16. Liquid quenched particle illustrating finer edges and near spherical dimensions.

In order to determine if the results obtained for the larger particles ("caps") were consistent, numerous additional particles burned. Most samples contained the products from one particle, however other samples were collected with multiple products.

Each pedestal containing the products from one aluminum particle had at least one particle with a mass mean diameter $\geq$ 42 microns. These particles all had a porous surface, while several had large craters in their surface caused possibly by an oxide lobe breaking free from the surface. A typical particle of this description is depicted in Figure 17 where the crater/cap was approximately 30 microns in diameter. To determine if this was a phenomenon of dry quenching, liquid-quenched particles were also measured. They had similar diameters and surface characteristics. Table 4 lists the particle sizes greater than 12 microns which were measured from numerous burning particles. A small percentage of the measured particles were in the range of 42 to 84 microns which could represent aluminum particles that burned with a single oxide lobe. The particles with diameters between 72 and 84 microns were almost certainly single oxide caps with diameters greater than 50 percent of the initial aluminum particle diameter. Over 90 percent of the larger particles had mean diameters between 12 and 36 microns. These particles were generally more "jagged" and non-spherical (Figures 15 and 16) and appeared to be oxide caps which had broken free from the larger particles as depicted in Figure 17. Since significantly different quench methods resulted in the same characteristics it is reasonable to assume that the oxide lobes were not removed during the quench process. These results imply that a burning aluminum particle, free-falling

with gravity acceleration, periodically sheds accumulated aluminum oxide fragments with diameters between 12 and 36 microns.

Particle Band	Percent in Band	Particle Band	Percent in Band	Particle Band	Percent in Band
12-18	32.2	36-42	0.00	60-66	0.00
18-24	23.7	42-48	5.10	66-72	0.00
24-30	15.3	48-54	0.00	72-78	3.40
30-36	15.3	54-60	1.70	78-84	3.40

Table 4. Measured particle "caps" from all tests.

Figure 17. Typical particle "cap" whose final diameter was a large fraction of its initial diameter.

V. SUMMARY AND CONCLUSIONS

The burning characteristics of aluminum particles were determined under atmospheric, gravity-fall conditions. Analysis of the residue indicated that the mass of aluminum oxide contained in particles larger than 12 microns was less than 25 percent, in good agreement with data reported from aluminized solid propellant. The measured particle size distributions and photomicrographs imply that the burning aluminum particles periodically expel aluminum oxide fragments with sizes between 14 and 36 microns.

LIST OF REFERENCES

Bartlett, R. W., and Delaney, L. J., "Effect of Liquid Surface Tension on Maximum Particle Size in Two-Phase Nozzle Flow," *Pyrodynamics*, vol. 4, pp. 337-341, 1966.

Bloomshield, F. S., Kraeutle, K. J., and Stalnaker, R. A., "Shuttle Redesign Solid Rocket Motor Aluminum Oxide Investigations," *21st JANNAF Exhaust Plume Technology Subcommittee Meeting, Sunnyvale, CA*, 19-21 October 1994.

Caveny, L. H., and Gany, A., "Breakup of Al/Al_2O_3 Agglomerates in Accelerating Flow Fields," AIAA-70-0300, *17th Aerospace Science Meeting at New Orleans, LA*, 15-17 January 1979.

Gomes, P. V., Roddenberry, D. S., Snaza, C. J., Yakin, B., Yi, C. M., and Netzer, D. W., "Nozzle geometry and Additive Effects on Plume Particulate Behavior in Subscale Solid Propellant Rocket Motors," *21st JANNAF Exhaust Plume Technology Subcommittee Meeting, Sunnyvale, CA*, CPIA Pub. 621, vol. 2, pp25-31, October 1994,.

Jenkins, R. M., and Hogland, R. F., "A Unified Theory of Particle Growth in Rocket Chambers and Nozzles," AIAA Paper No. 69-541, *5th Propulsion Joint Specialist Conference*, June 1969.

Laredo, D., McCrorie, J. D., Vaughn, J. K., and Netzer, D. W., "Motor and Plume Particle Size Measurements in Solid Propellant Micromotors," *Journal of Propulsion and Power, vol. 10, no. 3*, pp. 410-418, May-June 1994.

Pilch, M., and Erdman, C. A., "Use of Breakup Time Data and Velocity History Data to Predict the Maximum Size of Stable Fragments for Acceleration-Induced Breakup of a Liquid Drop," *International Journal of Multiphase Flow, vol. 13, no. 6,* pp. 74-757, 1987.

Price, E. W., Kraeutle, K. J., Prentice, J. L., Crump, J. E., and Zurn, D. E., *Behavior of Aluminum in Solid Propellant Combustion*, NWC TP 6120, Naval Weapons Center, China Lake, CA, March 1982.

Price, E. W., "Combustion of Metalized Propellants," *Fundamentals of Solid Propellant Combustion: Progress in Aeronautics and Astronautics, vol. 90*, edited by Kuo and Summerfield, AIAA, pp. 479-513, 1984.

Salita, Mark, "Survey of Recent Al_2O_3 Droplet Size Data in Solid Rocket Chambers, Nozzles, and Plumes," *21st JANNAF Exhaust Plume Technology Subcommittee Meeting, Sunnyvale, CA*, 19-21 October 1994.

Salita, M, "Predicted Slag Deposition Histories in Eight Solid Rocket Motors Using the CFD Model 'EVT'," AIAA-95-1728, *31st AIAA/ASME/SAE/ASEE Joint Propulsion Conference and Exhibit, San Diego, CA*, 10-12 July 1995.

Salita, Mark, "Workshop Report: Modeling of Slag Generation in Solid Rocket Motors," *30th Joint Propulsion Conference, Indianapolis, IN*, 26-27 June 1994.

INITIAL DISTRIBUTION LIST

1. Defense Technical Information Center 2
   8725 John J. Kingman Rd., STE 0944
   Ft. Belvoir, VA 22060-6218

2. Dudley Knox Library. 2
   Naval Postgraduate School
   411 Dyer Rd.
   Monterey, California 93943-5101

3. LT Eric C. Ruttenberg 3
   46588 Riverwood Terrace
   Sterling, VA 20165

4. Prof. David W. Netzer 2
   Code AA/Nt
   Naval Postgraduate School
   Monterey, CA 93943

5. Prof. Oscar Biblarz 1
   Code AA/Bi
   Naval Postgraduate School
   Monterey, CA 93943

6. Chairman 1
   Dept. of Aeronautics and Astronautics, Code AA
   Naval Postgraduate School
   Monterey, CA 93943